Published for SISSA by Springer

Received: December 17, 2024
Revised: February 19, 2025
Accepted: March 26, 2025
Published: May 2, 2025

Evidence of a CP broken deconfined phase in 4D SU(2) Yang-Mills theory at $\theta = \pi$ from imaginary θ simulations

Mitsuaki Hirasawa,[a,b] **Masazumi Honda**,[c,d,e] **Akira Matsumoto**,[c,d] **Jun Nishimura**[f,g] **and Atis Yosprakob**[h]

[a] *Department of Physics, University of Milano-Bicocca, Piazza della Scienza 3, I-20126 Milano, Italy*
[b] *Istituto Nazionale di Fisica Nucleare (INFN), Sezione di Milano-Bicocca, Piazza della Scienza 3, I-20126 Milano, Italy*
[c] *Yukawa Institute for Theoretical Physics, Kyoto University, Kitashirakawa Oiwakecho, Sakyo-ku, Kyoto 606-8502 Japan*
[d] *Interdisciplinary Theoretical and Mathematical Sciences Program (iTHEMS), RIKEN, 2-1 Hirosawa, Wako, Saitama 351-0198 Japan*
[e] *Graduate School of Science and Engineering, Saitama University, 255 Shimo-Okubo, Sakura-ku, Saitama 338-8570, Japan*
[f] *KEK Theory Center, High Energy Accelerator Research Organization (KEK), 1-1 Oho, Tsukuba, Ibaraki 305-0801, Japan*
[g] *Graduate Institute for Advanced Studies, SOKENDAI, 1-1 Oho, Tsukuba, Ibaraki 305-0801 Japan*
[h] *Department of Physics, Niigata University, 8050 Ikarashi, 2-no-cho, Nishi-ku, Niigata 950-2181 Japan*

E-mail: mitsuaki.hirasawa@mib.infn.it, masazumi.honda@yukawa.kyoto-u.ac.jp, akira.matsumoto@yukawa.kyoto-u.ac.jp, jnishi@post.kek.jp, ayosp@phys.sc.niigata-u.ac.jp

Abstract: The spontaneous breaking of CP symmetry in 4D SU(N) pure Yang-Mills theory at $\theta = \pi$ has recently attracted much attention in the context of the higher-form symmetry and the 't Hooft anomaly matching condition. Here we use Monte Carlo simulations to study the $N = 2$ case, which is interesting since it is the case opposite to the large-N limit, where explicit calculations are available. In order to circumvent the severe sign problem due to the θ term for real θ, we first obtain results at imaginary θ, where the sign problem is absent, and make an analytic continuation to real θ. We use the stout smearing in defining the θ term in the action to be used in our simulations. Thus we obtain the expectation value of the topological charge and the deconfining temperature at $\theta = \pi$, and provide evidence that the CP symmetry, which is spontaneously broken at low temperature, gets restored *strictly above* the deconfining temperature. This conclusion is consistent with the anomaly matching condition and yet differs from the prediction in the large-N limit.

https://doi.org/10.1007/JHEP05(2025)009

JHEP05(2025)009

Keywords: Lattice Quantum Field Theory, Non-Zero Temperature and Density, Spontaneous Symmetry Breaking

ArXiv ePrint: 2412.03683

JHEP05(2025)009

Contents

1 Introduction 1

2 How to probe the spontaneous CP symmetry breaking at $\theta = \pi$ 4

3 Definition of the topological charge on the lattice 6

4 Simulation results 9
- 4.1 θ dependence of the topological charge density 9
- 4.2 θ dependence of the deconfining temperature 16

5 Summary and discussions 17

A Derivation of the HMC force term with the stout smearing 18

1 Introduction

The topological aspect of quantum field theory has been one of the most important subjects in both particle physics and condensed matter physics. In particular, the dynamical effect of the topological θ term, which is purely non-perturbative, remains elusive due to the notorious sign problem in standard Monte Carlo methods.

In condensed matter physics, the θ parameter has been discussed intensively [1–10] in 2D O(3) non-linear sigma model, which is known as an effective model of the anti-ferromagnetic spin system. According to Haldane's conjecture [11, 12], this model is expected to be in a gapless phase at $\theta = \pi$, while it is in a gapped phase at $\theta = 0$.

In particle physics, the topological θ term may appear in 4D SU(N) Yang-Mills (YM) theory including QCD ($N = 3$), and it breaks CP symmetry in general. However, the experimental upper bound on the neutron electric dipole moment suggests that the θ parameter is unnaturally small as $|\theta| \lesssim 10^{-10}$ [13, 14], which is a naturalness problem known as the strong-CP problem. There have been many attempts to explain this either phenomenologically [15–20] or theoretically [21–23].

In fact, 4D SU(N) YM theory has CP symmetry not only at $\theta = 0$ but also at $\theta = \pi$ due to the 2π periodicity in θ. In particular, the CP symmetry at $\theta = \pi$ is considered to be spontaneously broken at low temperature, while it is known to be unbroken at sufficiently high temperature [24, 25]. Renewed interest in this issue has been triggered by recent developments in the higher-form symmetry [26] and the 't Hooft anomaly matching [27], which predict that, at $\theta = \pi$, either the CP or the $\mathbb{Z}_N$ center symmetry should be spontaneously broken unless the theory becomes gapless. Note here that the spontaneous breaking of the $\mathbb{Z}_N$ center symmetry corresponds to deconfinement. Therefore the prediction implies that the theory cannot be in a gapped confined phase without breaking the CP symmetry [28, 29]. In other words, the anomaly-matching condition claims that

$$T_{\rm CP} \geq T_{\rm dec}(\pi)\,, \tag{1.1}$$

JHEP05(2025)009

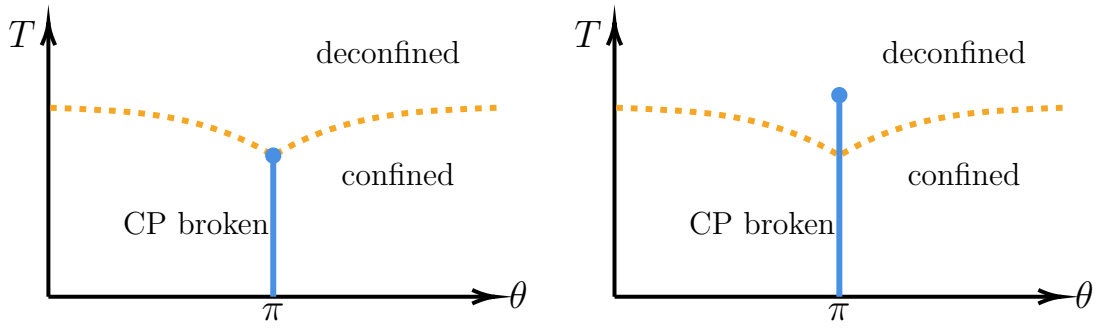

Figure 1. Two scenarios for the (θ, T)-phase diagram of 4D pure SU(N) Yang-Mills theory consistent with the anomaly matching condition. The blue solid line represents the first-order phase transition associated with the spontaneous breaking of CP symmetry. The orange dotted curve represents the deconfining transition that is believed to be of the first order for $N \geq 3$ and of the second order for $N = 2$. The left panel represents the scenario $T_{\rm CP} = T_{\rm dec}(\pi)$, while the right panel represents the scenario $T_{\rm CP} > T_{\rm dec}(\pi)$, which implies the existence of a deconfined phase with spontaneously broken CP symmetry.

where $T_{\rm CP}$ represents the temperature at which the CP symmetry at $\theta = \pi$ gets restored, and $T_{\rm dec}(\theta)$ represents the critical temperature of the deconfining transition, which depends on θ in general. Thus, an interesting question is whether CP restoration coincides with the deconfining transition ($T_{\rm CP} = T_{\rm dec}(\pi)$) or not ($T_{\rm CP} > T_{\rm dec}(\pi)$) as depicted in the Left and Right panels of figure 1, respectively. In particular, the second scenario implies the existence of a deconfined phase with spontaneously broken CP symmetry.

It is known that the first scenario is realized in the large-N limit [30, 31], where the CP symmetry at $\theta = \pi$ is spontaneously broken at low temperature, and it gets restored precisely at the deconfining temperature, at which the $\mathbb{Z}_N$ center symmetry gets spontaneously broken. Given the belief that the deconfining transition is of the first order for $N \geq 3$ and of the second order for $N = 2$, it was argued in ref. [28] that the first scenario is likely to be realized for $N \geq 3$ but not necessarily for $N = 2$. This issue has also been investigated in the SU(N) supersymmetric Yang-Mills theory (SYM) deformed by the gaugino mass and compactified on S^1 with periodic boundary conditions [32], which flows into the pure (non-supersymmetric) YM theory in the IR limit. Regarding the radius of S^1 as an analog of the inverse temperature, it was found that the phase diagram looks like figure 1 (Left) for $N \geq 3$, whereas for $N = 2$, it looks like figure 1 (Right), namely, there exists a CP-broken deconfined phase.[1] One should keep in mind, however, that the gaugino mass has to be small enough to make the analysis based on supersymmetry reliable. Note also that the radius of S^1 with periodic boundary conditions cannot be regarded as the inverse temperature, which actually requires anti-periodic boundary conditions for the gaugino field. Thus there is a strong motivation to investigate the phase diagram of 4D SU(N) pure YM theory with small N directly by numerical methods.

[1] It was pointed out [33] that this intermediate phase is analogous to the partially deconfined phase in large-N gauge theories, where the transition from the completely deconfined phase to the partially deconfined phase should be accompanied with the spontaneous breaking of the global symmetry, which is the CP symmetry in the present case.

JHEP05(2025)009

There are various approaches that have been proposed to overcome the sign problem caused by the θ term. In particular, the so-called subvolume method was applied to 4D SU(2) YM theory, where it was suggested that the CP symmetry at $\theta = \pi$ is broken at zero temperature and gets restored at $T_{\rm CP} \leq 1.2\, T_{\rm dec}(0)$ [34–36]. However, this does not tell us whether the inequality (1.1) is saturated or not. On the other hand, the density of states method (DOS) [37] and the complex Langevin method (CLM) [38] have been successfully applied to 2D U(1) gauge theory with the θ term using an open boundary condition. There are also some attempts to extend these works to 4D SU(2) YM theory [39, 40]. (See also ref. [41] for an earlier attempt to apply the CLM to 4D SU(3) YM theory.) The tensor renormalization group (TRG) [42, 43] has also been successfully applied to 2D U(1) gauge theory with the θ term, but treating a non-Abelian gauge group in TRG seems to be still difficult except in 2D [43–45]. (See, however, refs. [46–48] for recent developments.)

In our attempts [40] to extend our CLM work [38] on the 2D U(1) case with an open boundary to the 4D SU(2) case, we have found that the topological information leaks out from the open boundary by smearing, which was needed to define the topological charge unlike in the 2D U(1) case. Moreover, since the open boundary makes the topological charge non-integer, the 2π periodicity in θ is lost and the CP symmetry at $\theta = \pi$ is explicitly broken. In order to avoid these problems, we need to work with periodic boundary conditions, which would then cause either the topology freezing problem or the wrong convergence problem in the CLM depending on the coupling constant [38]. Thus simulating the theory directly at $\theta = \pi$ still remains a big challenge.

In this paper, we use yet another approach to the sign problem, which is based on analytic continuation from the imaginary θ region [49], where the sign problem is absent since the θ term becomes real.[2] This technique has been used to investigate the deconfining temperature [52–54], the free energy [55–57], the string tension, the glueball mass [58] and the electric dipole moment of the neutron [59, 60] as a function of θ in 4D SU(N) gauge theory for $N \geq 3$. Similarly, we calculate the expectation value of the topological charge at imaginary θ, and by fitting the results to an appropriate holomorphic function, we obtain $\langle Q \rangle_\theta$ at real θ through analytic continuation.[3] In particular, if the result of $\langle Q \rangle_\theta$ at $\theta = \pi$ is nonzero, it tells us that the CP symmetry is spontaneously broken. Unlike the previous imaginary θ simulations, we use the stout smearing [67] in defining the θ term in the action to be used in our simulation. This is of particular importance for our purpose since the CP symmetry at $\theta = \pi$ assumes that the topological charge takes integer values, which is not the case if one uses a naive definition.

We find that the CP symmetry is indeed spontaneously broken at low temperature. As we increase the temperature, the order parameter $\langle Q \rangle_{\theta=\pi}$ decreases and vanishes at some temperature $T_{\rm CP}$ close to $T_{\rm dec}(0)$. We also estimate the deconfining temperature $T_{\rm dec}(\theta)$ at

[2] This is analogous to the imaginary chemical potential approach [50, 51] to finite density QCD.

[3] In fact, imaginary θ enhances configurations with large topological charge, and hence it enables us to probe the tail of the topological charge distribution, which is difficult to determine otherwise. Then, by making a Fourier transform of the topological charge distribution, one can obtain the θ dependence of the partition function and hence the expectation value of the topological charge as well [61]. (See also ref. [62] for related work.) In fact, this method was applied to the Schwinger model [63] and the $\mathbb{CP}^{N-1}$ model [64–66]. It would be interesting to apply the same method to the 4D SU(2) YM case.

JHEP05(2025)009

real θ by analytic continuation, and find that $T_{\rm dec}(\pi) < T_{\rm dec}(0)$, which is consistent with the general expectation based on analytical studies [68–70] and numerical studies [52, 53, 71, 72]. Combining these results, we obtain the relation

$$T_{\rm CP} \sim T_{\rm dec}(0) > T_{\rm dec}(\pi)\,, \tag{1.2}$$

which suggests the existence of a CP-broken deconfined phase as in figure 1 (Right).

This paper is organized as follows. In section 2, we explain our strategy to probe the spontaneous CP symmetry breaking at $\theta = \pi$ by Monte Carlo simulations at imaginary θ. In section 3, we discuss the definition of the topological charge on the lattice based on the stout smearing, which we use in our Monte Carlo simulations. In section 4, we present our simulation results, which provide evidence of a CP broken deconfined phase. Section 5 is devoted to a summary and discussions. In appendix A, we derive the explicit form of the drift term, in the presence of the stout smearing, which is used in our simulation based on the hybrid Monte Carlo algorithm.

2 How to probe the spontaneous CP symmetry breaking at $\theta = \pi$

The 4D SU(N) gauge theory with the θ term is defined by the partition function

$$Z_\theta = \int \mathcal{D}A_\mu\, e^{-S_{\rm g} - i\theta Q}\,, \tag{2.1}$$

where $S_{\rm g}$ is the action for the gauge field A_μ, and Q is the topological charge defined by

$$Q = \frac{1}{32\pi^2}\epsilon_{\mu\nu\rho\sigma}\int d^4x \mathrm{Tr}\left(F_{\mu\nu}F_{\rho\sigma}\right)\,. \tag{2.2}$$

Under the CP transformation, the action $S_{\rm g}$ is invariant, whereas the topological charge Q flips its sign. On a compact manifold such as a 4D torus, the topological charge takes an integer value $Q \in \mathbb{Z}$, which implies the 2π periodicity under $\theta \mapsto \theta + 2\pi$. Therefore the theory has CP symmetry not only at $\theta = 0$ but also at $\theta = \pi$. The order parameter of spontaneous CP symmetry breaking at $\theta = \pi$ can be defined as

$$O = \lim_{\epsilon\to 0}\lim_{V\to\infty}\frac{\langle Q\rangle_{\theta=\pi-\epsilon}}{V}\,, \tag{2.3}$$

where V represents the space-time volume. It should be nonzero in the CP broken phase while it vanishes in the CP restored phase.

Note that the expectation value $\langle Q\rangle_\theta$ has the following property around $\theta = \pi$

$$\langle Q\rangle_{\theta=\pi-\epsilon} = -\langle Q\rangle_{\theta=-(\pi-\epsilon)} = -\langle Q\rangle_{\theta=\pi+\epsilon}\,, \tag{2.4}$$

where we use the CP symmetry and the 2π periodicity under $\theta \mapsto \theta + 2\pi$ in the first and second equalities, respectively. This implies that $\lim_{V\to\infty}\frac{\langle Q\rangle_\theta}{V}$ changes discontinuously at $\theta = \pi$ in the CP broken phase while it is continuous at $\theta = \pi$ in the CP restored phase. Thus, the spontaneous CP symmetry breaking at $\theta = \pi$ implies the existence of a first-order phase transition at $\theta = \pi$.

JHEP05(2025)009

Unfortunately, the spontaneous CP symmetry breaking at $\theta = \pi$ is difficult to study by Monte Carlo simulations due to the sign problem as one can see from (2.1), where the θ term appears as a pure phase factor in the integrand. In order to motivate our strategy, let us consider the topological charge distribution

$$\rho(q) = \frac{1}{Z_0} \int \mathcal{D}A_\mu \, \delta(q - Q) \, e^{-S_g} \,, \tag{2.5}$$

which can be calculated by Monte Carlo simulations at $\theta = 0$ without the sign problem. Note that $\rho(q)$ is an even function, i.e., $\rho(q) = \rho(-q)$ due to CP symmetry. Using this distribution, the partition function (2.1) can be written as

$$Z_\theta = Z_0 \int dq \, e^{-i\theta q} \, \rho(q) \,, \tag{2.6}$$

which implies that Z_θ may be regarded as the Fourier transform of the topological charge distribution $\rho(q)$ at $\theta = 0$. Note also that the expectation value of the topological charge can be written as

$$\langle Q \rangle_\theta = i \frac{\partial}{\partial \theta} \log Z_\theta = \frac{\int dq \, q \, e^{-i\theta q} \, \rho(q)}{\int dq \, e^{-i\theta q} \, \rho(q)} \,. \tag{2.7}$$

Hence one can obtain $\langle Q \rangle_\theta$ if $\rho(q)$ is known and vice versa.

There are actually known results in two simplified cases. One is the result obtained by the instanton gas approximation [24, 25], which is considered to be valid at sufficiently high temperature. The other is the result obtained in the large-N limit [30, 31] at low temperature, where the topological charge distribution is known to be Gaussian. The quantity $\langle Q \rangle_\theta$ in these two cases is given as

$$\frac{\langle Q \rangle_\theta}{V} = \begin{cases} i\chi_0 \sin\theta \, : & \text{instanton gas approximation (high } T) \,, \\ i\chi_0 \, \theta \quad : & \text{large-}N \text{ limit (low } T) \,, \end{cases} \tag{2.8}$$

for $|\theta| < \pi$, where χ_0 is the topological susceptibility at $\theta = 0$ defined by

$$\chi_0 = \frac{i}{V} \frac{\partial}{\partial \theta} \langle Q \rangle_\theta \Big|_{\theta=0} = \frac{1}{V} \left\{ \langle Q^2 \rangle_0 - (\langle Q \rangle_0)^2 \right\} \,. \tag{2.9}$$

This implies that the CP symmetry is spontaneously broken at low T, whereas it gets restored at high T in these simplified cases. Using (2.7), we obtain the asymptotic behavior of the topological charge distribution $\rho(q)$ at large $|q|$ as

$$\rho(q) \sim \begin{cases} \exp\Big(- |q| \log |q| \Big) \, : & \text{instanton gas approximation (high } T) \,, \\ \exp\Big(-\frac{q^2}{2\chi_0 V} \Big) \quad : & \text{large-}N \text{ limit (low } T) \,. \end{cases} \tag{2.10}$$

This suggests that the spontaneous breaking of the CP symmetry at $\theta = \pi$ is related to the asymptotic behavior of $\rho(q)$. In figure 2, we plot $\rho(q)$ against q in the logarithmic scale for the two cases. We can see a clear difference in the tail of the distribution, which is difficult to probe by Monte Carlo simulations at $\theta = 0$, however.

JHEP05(2025)009

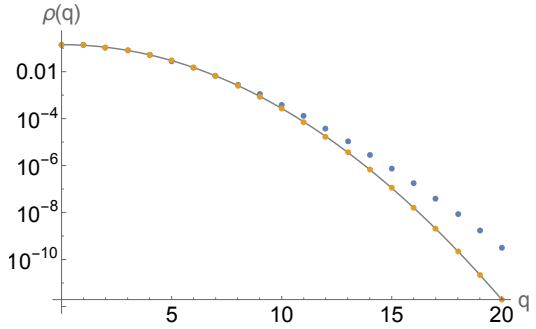

Figure 2. The topological charge distribution is plotted in the logarithmic scale for the result obtained by the instanton gas approximation (blue) and that obtained in the large-N limit at low temperature (orange). The solid line represents a Gaussian behavior $\propto \exp\left(-q^2/2\chi_0 V\right)$ known for the latter case.

Let us here recall that Monte Carlo simulations can be performed for imaginary θ since the sign problem is absent there. Note, in particular, that the phase factor $e^{-i\theta Q}$ becomes a weight $e^{\tilde{\theta}Q}$ with $\tilde{\theta} = -i\theta \in \mathbb{R}$ in that case. This makes it possible to probe the topological charge distribution $\rho(q)$ at large $|q|$. In the above two simplified cases, the expectation value $\langle Q \rangle_{i\tilde{\theta}}$ becomes

$$\frac{\langle Q \rangle_{i\tilde{\theta}}}{V} = \begin{cases} \chi_0 \sinh\tilde{\theta} : \text{ instanton gas approximation (high } T\text{)}, \\ \chi_0\,\tilde{\theta} \quad\quad : \text{ large-}N\text{ limit (low } T\text{)}. \end{cases} \tag{2.11}$$

The different asymptotic behaviors of the topological charge distribution correspond here to the different growths of $\langle Q \rangle_{i\tilde{\theta}}$ at large $\tilde{\theta}$. In general, we expect exponential growth for the CP-restored phase and power-law growth for the CP broken phase. This is the basic strategy we adopt in this work.

3 Definition of the topological charge on the lattice

In this section, we define the gauge theory on the lattice, which we simulate by the standard hybrid Monte Carlo method. In particular, we define the topological charge carefully using the so-called stout smearing.

The action for the gauge field $S_{\rm g}$ in (2.1) is represented on the lattice by the standard Wilson plaquette action as

$$S[U] = -\frac{\beta}{2N}\sum_n \sum_{\mu\neq\nu} \mathrm{Tr}\left\{P_n^{\mu\nu}(U)\right\}\,, \tag{3.1}$$

where the plaquette $P_n^{\mu\nu}(U)$ is defined by

$$P_n^{\mu\nu}(U) = U_{n,\mu}U_{n+\mu,\nu}U^\dagger_{n+\nu,\mu}U^\dagger_{n,\nu}\,. \tag{3.2}$$

In this work, we use the $L_{\rm s}\times L_{\rm s}\times L_{\rm s}\times L_{\rm t}$ lattice with various $16 \le L_{\rm s} \le 64$ fixing $L_{\rm t} = 5$.

Since we use fixed $L_{\rm t} = 5$, we change the temperature $T = 1/(aL_{\rm t})$ by changing the lattice spacing a, which amounts to changing β. To be concrete, we use the relationship

JHEP05(2025)009

between the temperature and β given in ref. [73] as

$$\frac{T}{T_c} = \frac{1}{t_c L_t} \exp\left(\frac{51}{121} \log \frac{11}{6\pi^2\beta} + \frac{3\pi^2\beta}{11} - c_3 \frac{18432\pi^4}{121\beta^3} \right) , \tag{3.3}$$

where T_c is the deconfining temperature in the continuum limit, $t_c = 21.45(14)$, and $c_3 = 5.529(63) \times 10^{-4}$. The value of β corresponding to each T/T_c is given in table 1.

A naive definition of the topological charge $Q(U)$ on the lattice is given by [74]

$$Q(U) = -\frac{1}{32\pi^2} \sum_n \frac{1}{2^4} \sum_{\mu,\nu,\rho,\sigma=\pm1}^{\pm4} \tilde{\epsilon}_{\mu\nu\rho\sigma} \mathrm{Tr}\left(P_n^{\mu\nu} P_n^{\rho\sigma}\right) , \tag{3.4}$$

where $\tilde{\epsilon}_{\mu\nu\rho\sigma}$ is the totally anti-symmetric tensor satisfying $\tilde{\epsilon}_{(-\mu)\nu\rho\sigma} = -\epsilon_{\mu\nu\rho\sigma}$. While this quantity reproduces the topological charge in the continuum limit, it typically has severe lattice artifacts, which obscure the topological nature. In order to recover the topological nature even at finite lattice spacing, we remove the high momentum modes in each configuration by applying the stout smearing [67].

Here we briefly review the procedure. The original configuration $U_{n,\mu}$ is replaced with the smeared configuration $\tilde{U}_{n,\mu}$ obtained by N_ρ steps of the stout smearing as

$$(U_{n,\mu} \equiv) U_{n,\mu}^{(0)} \to U_{n,\mu}^{(1)} \to \cdots \to (\tilde{U}_{n,\mu} \equiv) U_{n,\mu}^{(N_\rho)} , \tag{3.5}$$

where each step is defined by

$$U_{n,\mu}^{(k+1)} = \exp\left(iY_{n,\mu}^{(k)}\right) U_{n,\mu}^{(k)} , \tag{3.6}$$

$$iY_{n,\mu}^{(k)} = -\frac{\rho}{2} \mathrm{Tr}\left(J_{n,\mu}^{(k)} \tau^a\right) \tau^a = -\frac{\rho}{2} \left\{ J_{n,\mu}^{(k)} - \frac{1}{2} \mathrm{Tr}\left(J_{n,\mu}^{(k)}\right) \mathbb{1} \right\} , \tag{3.7}$$

$$J_{n,\mu}^{(k)} = U_{n,\mu}^{(k)} \Omega_{n,\mu}^{(k)} - \Omega_{n,\mu}^{(k)\,\dagger} U_{n,\mu}^{(k)\,\dagger} , \tag{3.8}$$

$$\Omega_{n,\mu}^{(k)} = \sum_{\sigma(\neq\mu)} \left(U_{n+\hat{\mu},\sigma}^{(k)} U_{n+\hat{\sigma},\mu}^{(k)\dagger} U_{n,\sigma}^{(k)\dagger} + U_{n+\hat{\mu}-\hat{\sigma},\sigma}^{(k)\dagger} U_{n-\hat{\sigma},\mu}^{(k)\dagger} U_{n-\hat{\sigma},\sigma}^{(k)} \right) . \tag{3.9}$$

We have defined the SU(2) generators τ^a with the normalization $\mathrm{tr}\left(\tau^a \tau^b\right) = \frac{1}{2}\delta_{ab}$. The smearing parameter $\rho > 0$ in (3.7) should be chosen appropriately as we discuss shortly. Note that the stout smearing is nothing but the discretized version of the gradient flow method [75] since $J_{n,\mu}^{(k)}$ represents the derivative of the Wilson plaquette action with respect to the link variable $U_{n,\mu}^{(k)}$. One of the biggest advantages of the stout smearing among various smearing techniques is that the smeared link is differentiable with respect to the original link, which is crucial in applying the HMC algorithm to the action including a term defined with the smeared link.

In the SU(2) case, since the eigenvalues of the traceless Hermitian matrix $Y_{n,\mu}$ are given by $\pm\kappa_{n,\mu}$ with

$$\kappa_{n,\mu} = \sqrt{\frac{1}{2} \mathrm{Tr}(Y_{n,\mu})^2} , \tag{3.10}$$

the matrix $\exp(iY_{n,\mu})$ in (3.6) can be obtained easily by

$$\exp(iY_{n,\mu}) = (\cos\kappa_{n,\mu})\mathbb{1} + \frac{\sin\kappa_{n,\mu}}{\kappa_{n,\mu}} iY_{n,\mu} . \tag{3.11}$$

JHEP05(2025)009

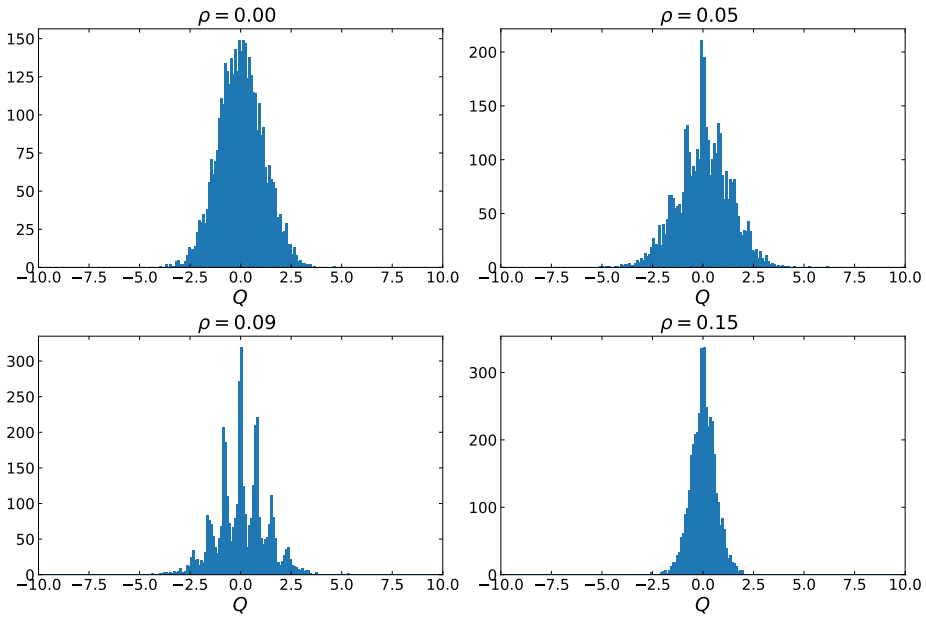

Figure 3. The histogram of the topological charge after the stout smearing for $\rho = 0$, 0.05, 0.09, and 0.15 with the fixed number of smearing steps $N_\rho = 40$. The lattice volume is $V_{\rm L} = 20^3 \times 5$, and the temperature is $T = 1.2\,T_{\rm c}$.

In figure 3, we plot the distribution of the topological charge $Q[\tilde{U}]$ computed from the smeared link variables $\tilde{U}_{n,\mu}$ at $\theta = 0$ for various ρ with the fixed number of smearing steps $N_\rho = 40$. We find that a comb-like structure is most clearly seen for $\rho = 0.09$. Therefore, we use $N_\rho = 40$ and $\rho = 0.09$ in our simulation.

Note that the positions of the peaks are slightly shifted from integer values due to the lattice artifacts. It is well known that one can actually make the position of the peaks closer to integers by rescaling $Q \to wQ$ with some parameter $w > 0$. (See, for instance, ref. [76].) In this work, we numerically determine the value of w from $Q[\tilde{U}]$ obtained for each configuration in such a way that the cost function

$$F(w) = \left\langle 1 - \cos\Big(2\pi w Q[\tilde{U}]\Big) \right\rangle \tag{3.12}$$

is minimized, where the symbol $\langle \cdots \rangle$ represents the ensemble average. (A similar cost function has been used in ref. [56], for instance.) In practice, we calculate $F(w)$ as a function of w, and determine the optimal value $w_{\rm opt}$ by fitting the result to $F(w) = A(w - w_{\rm opt})^2 + B$ near the minimum.

In table 1, we present the optimal value of w obtained in this way for $L = 16$ at each temperature. For a larger lattice at low temperature, it turns out to be difficult to find the minimum since the comb-like structure becomes unclear. On the other hand, at high temperature, we find that the optimal value of w is actually almost independent of the volume. Therefore, we use the values in table 1 for all $L_{\rm s}$.

In our simulation, the topological charge is defined by $\tilde{Q} \equiv wQ[\tilde{U}]$ with the smeared link variables $\tilde{U}_{n,\mu}$, whereas the plaquette action is defined with the original link variables $U_{n,\mu}$.

JHEP05(2025)009

T/T_c	β	w
0.90	2.33381	1.2234(3)
0.96	2.35320	1.2176(3)
0.98	2.35943	1.2167(1)
0.99	2.36250	1.2183(4)
1.00	1.36554	1.2183(1)

T/T_c	β	w
1.01	2.36856	1.2200(3)
1.02	2.37155	1.2217(3)
1.03	2.37452	1.2233(2)
1.04	2.37745	1.2247(2)
1.10	2.39458	1.2431(1)

Table 1. The value of β in the Wilson plaquette action (3.1) used in our simulations is given at each temperature based on the relation (3.3). We also present the rescaling factor w that makes the topological charge close to integers at each temperature for $L_s = 16$.

We will denote $\tilde{Q}$ simply as Q in what follows. In appendix A, we review how to calculate the force term in the hybrid Monte Carlo algorithm with the stout smearing.

4 Simulation results

In this section, we present our results of the Monte Carlo simulation. We compute the topological charge $\langle Q\rangle_{i\tilde{\theta}}$ and fit the result to some holomorphic function of $\tilde{\theta}$. By making an analytic continuation of the fitting functions, we obtain $\langle Q\rangle_\theta$ for real θ and determine whether the CP symmetry is spontaneously broken or not at each temperature, which tells us the critical temperature $T_{\rm CP}$ for the spontaneous CP symmetry breaking. We also determine $T_{\rm dec}(\theta)$ by analytical continuation and show that $T_{\rm CP} > T_{\rm dec}(\pi)$.

In order to justify the application of analytic continuation, $\langle Q\rangle_\theta$ has to be an analytic function of θ, which cannot be true in the rigorous sense since there is a deconfining phase transition as one increases θ at some temperature fixed in a certain range. (See figure 1.) However, in the present case of the SU(2) YM theory, the deconfining phase transition is of the second order[4] and hence $\langle Q\rangle_\theta$ is continuous across the transition as a function of θ. Here we assume that it is not only continuous but also analytic across the transition within small errors given that the non-analytic behavior at a second order transition is observed only in a detailed analysis of finite volume effects close to the transition. Indeed this assumption seems to be valid at least in the imaginary θ region that can be directly explored by our simulations. (See the last paragraph of section 4.2.) Under this assumption, it is expected that the analytic continuation is valid until one hits the first-order phase transition line at $\theta = \pi$ if it exists.

4.1 θ dependence of the topological charge density

In figure 4, we plot the topological charge density $\langle Q\rangle_{i\tilde{\theta}}/V_s$ against $\tilde{\theta}$ for $L_s = 16, 20, 24$ with fixed $L_t = 5$. For each $\tilde{\theta}$, we fit the data points to the linear function $f(V_s) = c + b/V_s$, where c and b are the fitting parameters and $V_s = L_s^3$ is the spatial lattice volume. The results obtained by the $L_s \to \infty$ extrapolation are shown in the same figure.

[4]In the case of the SU(3) YM theory, the deconfining phase transition is of the first order, which implies that $\langle Q\rangle_\theta$ is no longer continuous across the transition. Thus, for the temperature at which the deconfining phase transition occurs at some θ, the analytic continuation with respect to θ cannot be extended further. The spontaneous CP symmetry breaking can still be investigated outside this temperature region.

JHEP05(2025)009

T/T_c	χ_0	χ^2/N_{DF}
0.90	0.000351(1)	0.60
0.96	0.000291(1)	2.37
0.98	0.000277(2)	0.53
0.99	0.000268(1)	0.75
1.00	0.000258(2)	1.67

T/T_c	χ_0	χ^2/N_{DF}
1.01	0.000243(1)	2.12
1.02	0.000228(2)	2.25
1.03	0.000209(2)	2.91
1.04	0.0001917(9)	1.78
1.10	0.0001171(5)	0.98

Table 2. The topological susceptibility χ_0 in the lattice unit after the infinite volume extrapolation for various temperature within $0.9 \leq T/T_c \leq 1.1$.

Next, we show our results[5] for the topological susceptibility χ_0 at $\theta = 0$, which is defined by (2.9). From now on, we assume that χ_0 is made dimensionless by using the lattice unit. In figure 5, the topological susceptibility χ_0 is plotted against $1/V_s$ for $16 \leq L_s \leq 64$. The natural fitting functions are[6]

$$f_{\rm low}(L_s) = c_0 + c_1 e^{-c_2 L_s} \qquad \text{for } T \leq T_c\,, \tag{4.1}$$

$$f_{\rm high}(V_s) = d_0 + d_1/V_s \qquad \text{for } T > T_c\,, \tag{4.2}$$

where c_0, c_1, c_2, d_0 and d_1 are the fitting parameters. The values of χ_0 after the infinite volume extrapolation are shown in table 2. In figure 5, we show the fitting curves for both functions (4.1) and (4.2) at each temperature for comparison. We find that the choice of the fitting function does not affect the extrapolated values beyond the fitting errors.

Using the results for the topological charge density and the topological susceptibility after the infinite volume extrapolation, we determine the holomorphic function that describes the $\tilde{\theta}$ dependence of the topological charge density as follows. According to our discussions in section 2, a natural ansatz for $\frac{1}{V_s}\langle Q\rangle_\theta$ in the real θ region within $|\theta| < \pi$ is[7]

$$\begin{aligned} g(\theta) &= -i(a_1\theta + a_3\theta^3 + a_5\theta^5) && \text{in the CP broken phase}\,, \\ h(\theta) &= -i(b_1 \sin\theta + b_2 \sin 2\theta + b_3 \sin 3\theta) && \text{in the CP restored phase}\,, \end{aligned} \tag{4.3}$$

respectively, where we have taken into account the fact that the topological charge is a CP-odd quantity. We find that adding more terms in the expansion causes overfitting and hence the truncation at this order seems to be optimal.[8]

Using the topological susceptibility χ_0 at $\theta = 0$ after the infinite volume extrapolation, we get the constraints $a_1 = \chi_0$ and $b_1 + 2b_2 + 3b_3 = \chi_0$, which can be used to reduce the

[5] Since this only requires simulations at $\tilde{\theta} = 0$, which is much cheaper than simulations at $\tilde{\theta} \neq 0$, we were able to obtain many data points within $16 \leq L_s \leq 64$.

[6] The reason for this choice is that the nonzero glueball mass leads to an exponentially fast approach to the infinite volume limit in the confined phase [77]. On the other hand, the glueball contribution is expected to be suppressed in the deconfined phase, and therefore the leading finite volume effect is expected to be proportional to $1/V_s$ there. In the temperature region investigated in this work, however, the extrapolation does not depend much on this choice.

[7] Note, in particular, that the function $h(\theta)$ includes the behavior $\langle Q\rangle \propto \sin\theta$ obtained by the dilute instanton gas approximation, which is expected to be valid at sufficiently high temperature [24, 25].

[8] This applies to the fitting ansatz (4.7) as well.

JHEP05(2025)009

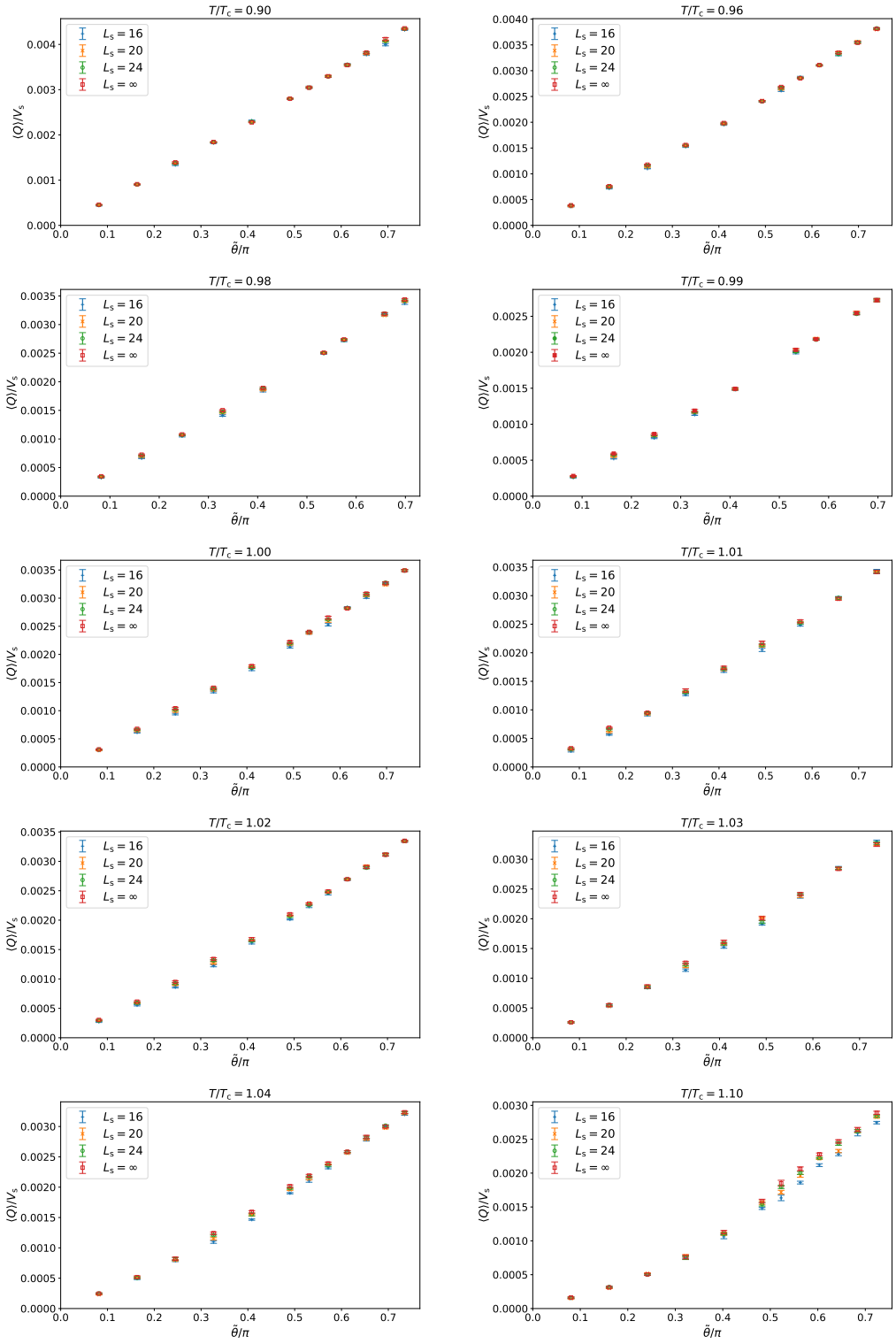

Figure 4. The topological charge density $\langle Q \rangle_{i\tilde{\theta}} / V_s$ is plotted against $\tilde{\theta}/\pi$ for $L_s = 16, 20, 24$ at various temperature within $0.9 \leq T/T_c \leq 1.1$. The results of the infinite volume extrapolation are plotted as well.

JHEP05(2025)009

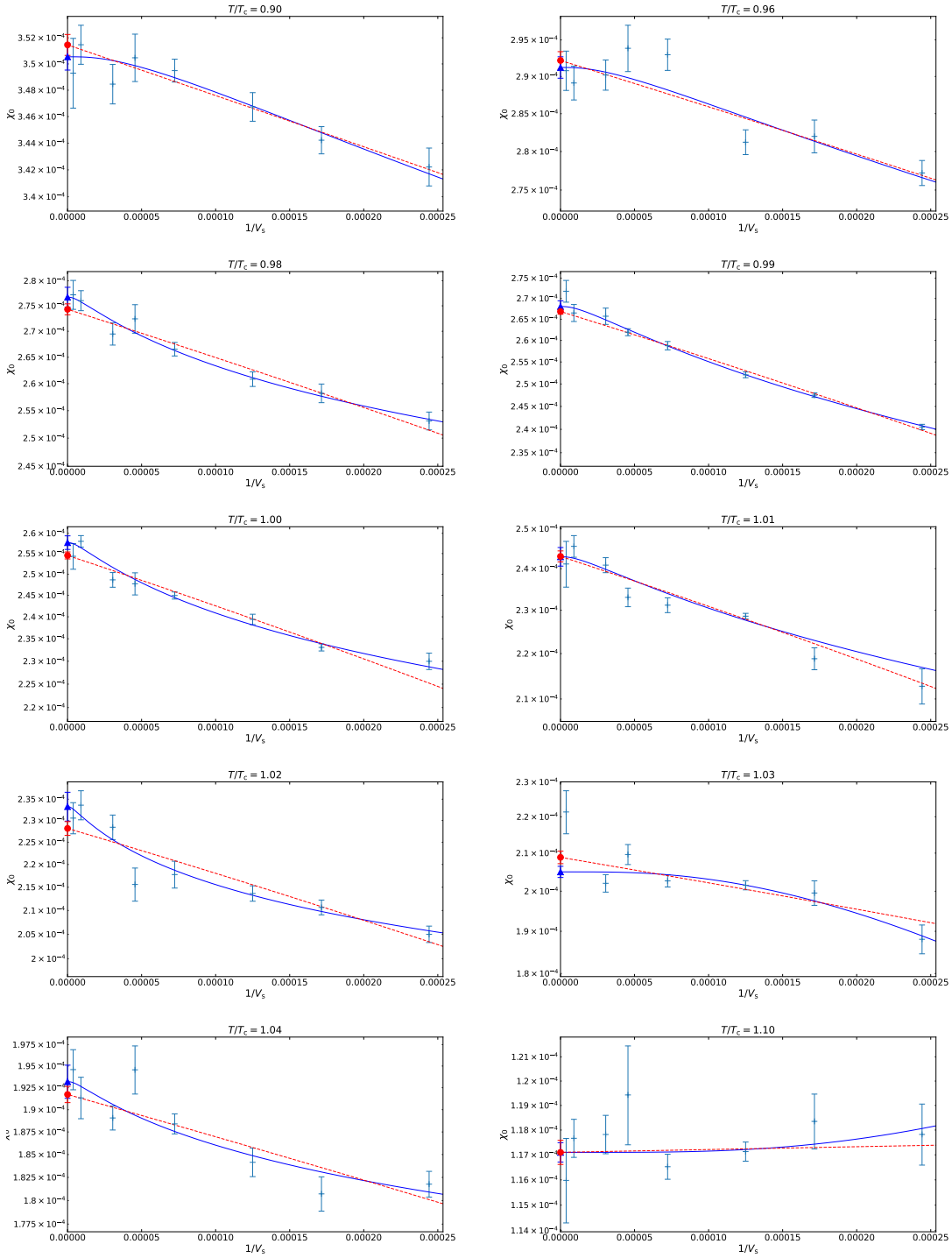

Figure 5. The topological susceptibility χ_0 in the lattice unit is plotted against $1/V_s$. The blue solid lines represent fits to the function (4.1), while the red dashed lines represent fits to the function (4.2). The blue triangles and the red circles represent the corresponding extrapolated values of χ_0 at each temperature.

JHEP05(2025)009

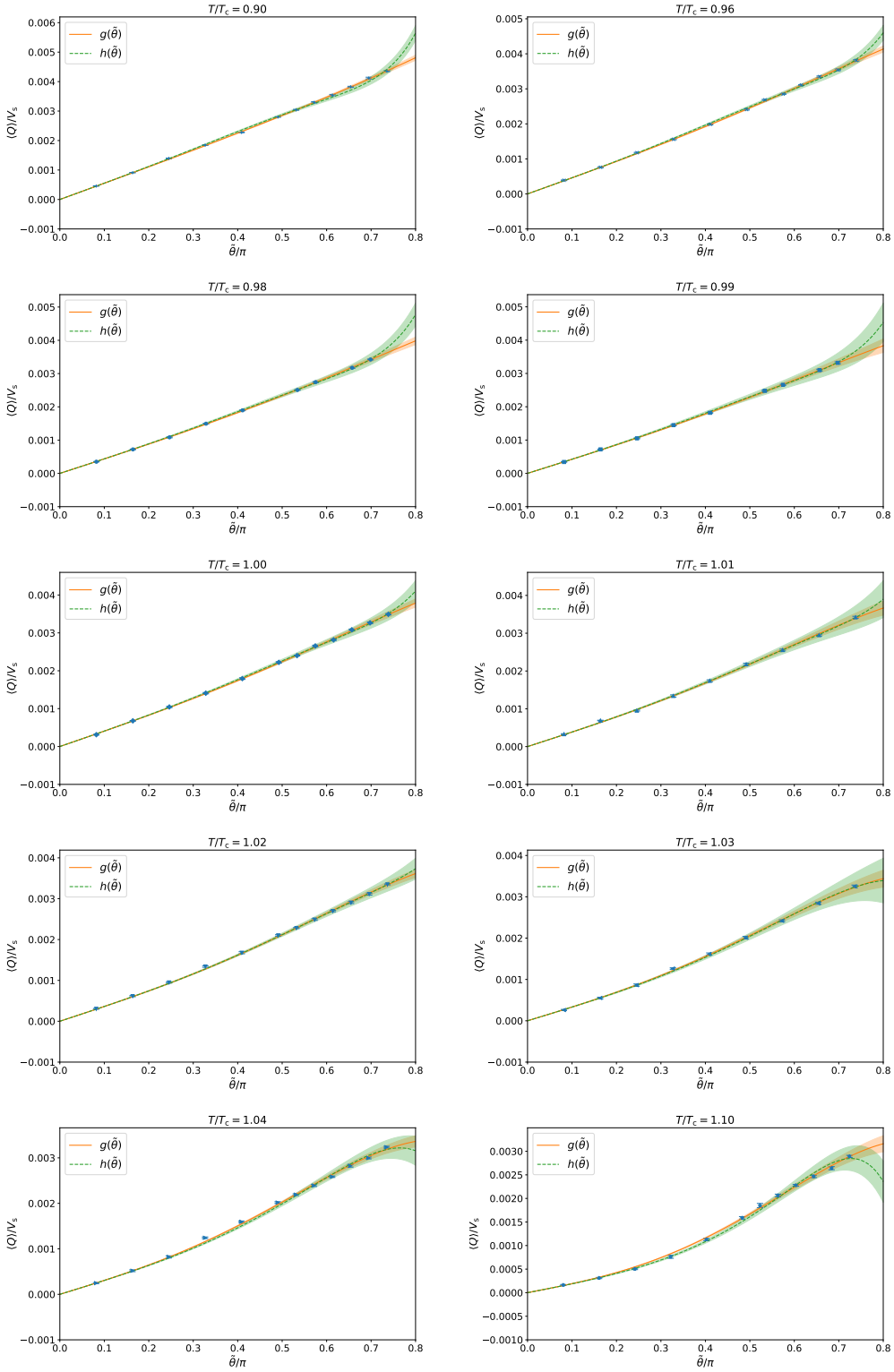

Figure 6. The topological charge density $\langle Q \rangle_{i\tilde{\theta}} / V_s$ after the infinite volume extrapolation is plotted against $\tilde{\theta}/\pi$ at various temperature within $0.9 \leq T/T_c \leq 1.1$. We fit the data points to the functions (4.4) (orange curve) and (4.5) (green curve) at each temperature. The values of the fitting parameters are given in table 3. The error bands are also shown with light colors.

JHEP05(2025)009

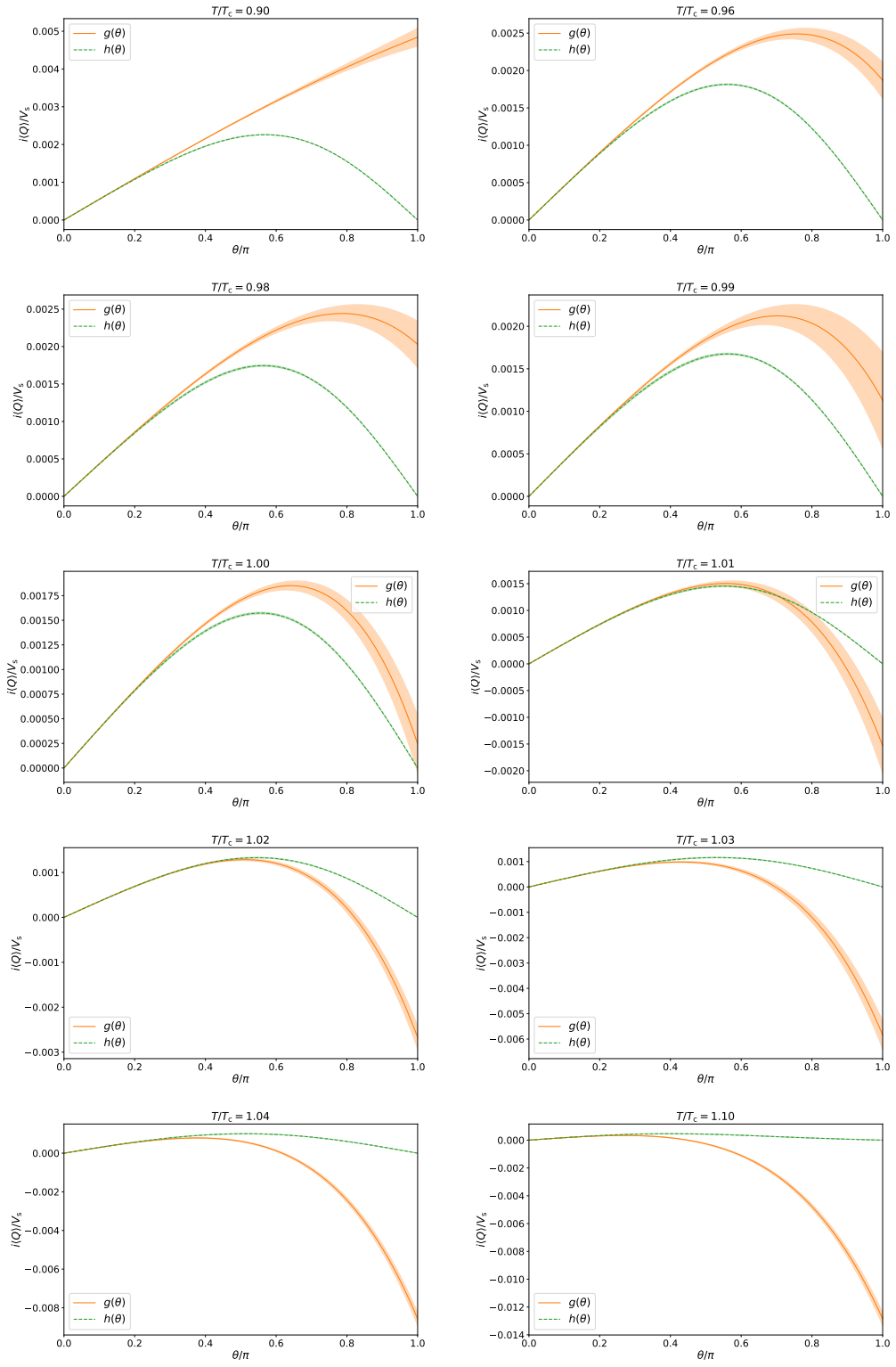

Figure 7. The topological charge density $\lim_{V_s\to\infty} i\langle Q\rangle_\theta / V_s$ for real θ obtained by analytic continuation of the fitting functions is plotted against θ/π at various temperature within $0.9 \leq T/T_c \leq 1.1$. The orange and green curves correspond to the functions $g(\theta)$ and $h(\theta)$ in (4.3), respectively. The error bands are also shown with light colors.

JHEP05(2025)009

	polynomial			hyperbolic sine		
T/T_c	a_3	a_5	$\chi^2/N_{\rm DF}$	b_2	b_3	$\chi^2/N_{\rm DF}$
0.90	0.0007(1)	0.0001(2)	1.92	-0.000249(2)	0.0000117(2)	16.14
0.96	0.00162(9)	-0.0011(2)	2.63	-0.000177(2)	0.0000076(2)	5.12
0.98	0.0015(1)	-0.0008(3)	0.92	-0.000179(3)	0.0000084(3)	1.74
0.99	0.0018(2)	-0.0013(5)	1.42	-0.000166(4)	0.0000075(4)	1.92
1.00	0.0021(1)	-0.0017(3)	1.55	-0.000141(2)	0.0000056(2)	2.33
1.01	0.0028(2)	-0.0025(5)	7.73	-0.000118(4)	0.0000043(3)	6.92
1.02	0.0033(1)	-0.0029(2)	2.18	-0.000094(2)	0.0000030(2)	1.68
1.03	0.0045(2)	-0.0046(5)	1.46	-0.000056(4)	0.0000006(4)	2.48
1.04	0.0057(1)	-0.0059(3)	5.10	-0.000021(3)	-0.0000015(2)	11.29
1.10	0.0077(2)	-0.0069(4)	2.67	0.000092(3)	-0.0000077(3)	4.26

Table 3. The values of the fitting parameters obtained by fitting $\langle Q\rangle_{i\tilde{\theta}}/V_{\rm s}$ after the infinite volume extrapolation at various temperature within $0.9 \leq T/T_{\rm c} \leq 1.1$.

number of fitting parameters. Thus, we obtain the ansatz for imaginary $\theta = i\tilde{\theta}$

$$g(i\tilde{\theta}) = \chi_0\tilde{\theta} - a_3\tilde{\theta}^3 + a_5\tilde{\theta}^5\,, \tag{4.4}$$

$$h(i\tilde{\theta}) = (\chi_0 - 2b_2 - 3b_3)\sinh\tilde{\theta} + b_2\sinh 2\tilde{\theta} + b_3\sinh 3\tilde{\theta}\,. \tag{4.5}$$

In figure 6, we fit our data points to (4.4) (orange curve) and (4.5) (green curve) at various temperature within $0.9 \leq T/T_{\rm c} \leq 1.1$. The values of the fitting parameters and the normalized chi-square $\chi^2/N_{\rm DF}$ are given in table 3. We find at lower temperature $T/T_{\rm c} \leq 1.0$ that the fitting to (4.5) is not good, which suggests that the system is in the CP broken phase. On the other hand, at higher temperature $T/T_{\rm c} \geq 1.01$, the normalized chi-square $\chi^2/N_{\rm DF}$ turns out to be large for both ansatzes, which may be due to a few data points around the deconfining phase transition at $\tilde{\theta} = \tilde{\theta}_{\rm c}$. (See the last paragraph of section 4.2.) Therefore, in the following analysis, we focus on the fitting curve obtained at lower temperature $T/T_{\rm c} \leq 1.0$ with the fitting ansatz (4.4).

In figure 7, we plot the fitting functions (4.3) after the analytic continuation. The orange and green curves correspond to $g(\theta)$ and $h(\theta)$, respectively. To determine the CP restoration temperature, we focus on the curve corresponding to the function $g(\theta)$ in the low temperature region. As the temperature is increased, the curve starts to bend and the gap at $\theta = \pi$ disappears around $T/T_{\rm c} \sim 1.0$, which we identify as the CP restoration temperature $T_{\rm CP}$. Based on this, we arrive at the prediction for $\frac{1}{V_s}\langle Q\rangle_\theta$ in figure 8, where we plot the function $g(\theta)$ for $T/T_{\rm c} \leq 1.00$ and the function $h(\theta)$ for $T/T_{\rm c} \geq 1.01$.

JHEP05(2025)009

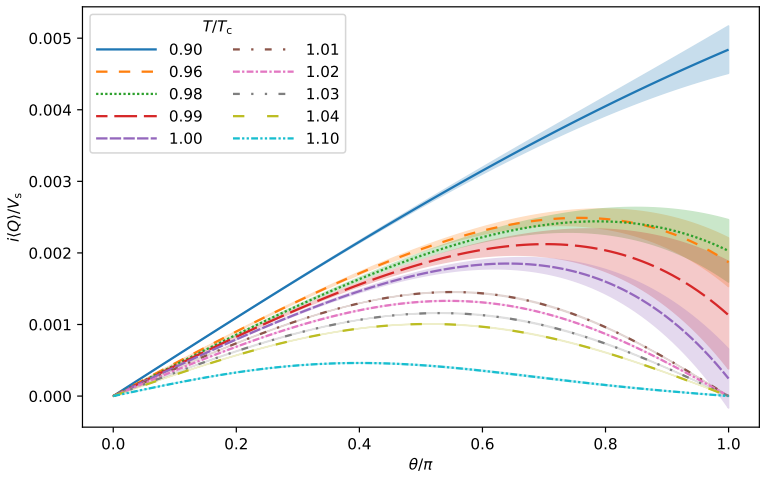

Figure 8. Our prediction for $\lim_{V_s\to\infty} i\,\langle Q\rangle_\theta\,/V_s$ is plotted against θ/π at various temperature within $0.9 \le T/T_c \le 1.1$. The gap at $\theta = \pi$ disappears at some T within $1.0 \lesssim T/T_c \lesssim 1.01$.

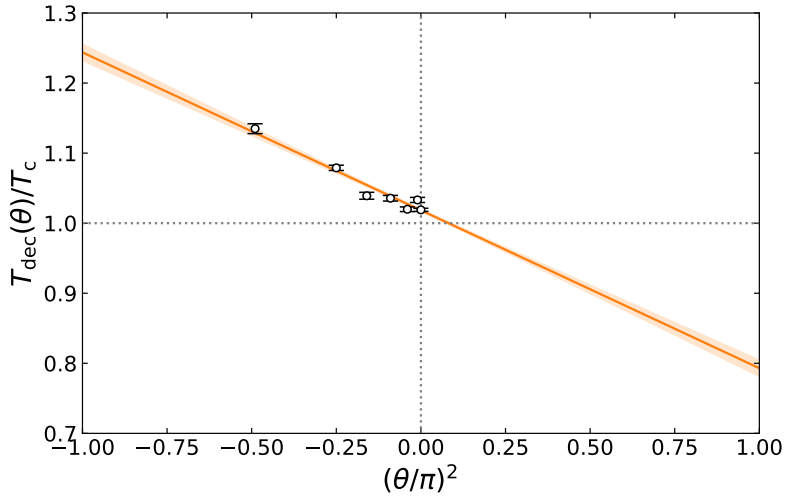

Figure 9. The deconfining temperature after the infinite volume extrapolation is plotted against $(\theta/\pi)^2$. The curves represent the fit to the function (4.7).

4.2 θ dependence of the deconfining temperature

In order to investigate the inequality (1.1), we still have to determine $T_{\rm dec}(\pi)$ that appears on the right-hand side. For that, we discuss the θ dependence of the deconfining temperature,[9] again by analytic continuation from the results obtained at imaginary θ. Note that in pure SU(N) Yang-Mills theory that we are dealing with, the Polyakov loop is an order parameter

[9]When this paper was about to be completed, we encountered a preprint [78], which addresses this issue using the subvolume method. The deconfinement temperatures obtained at real θ in that paper lie close to the fitting curve in our figure 9.

JHEP05(2025)009

for the spontaneous $\mathbb{Z}_N$ center symmetry breaking, which corresponds to the deconfining phase transition. Therefore we expect to observe a peak in the corresponding susceptibility at the deconfining temperature.

In order to determine $T_{\rm dec}$ at imaginary θ, we measure the Polyakov loop susceptibility $\chi_{\rm P}(T)$ at various temperature and fit our results to the Lorentzian function

$$\chi_{\rm P}(T) = \frac{A}{(T - T_{\rm peak})^2 + w^2}\,, \tag{4.6}$$

where A, $T_{\rm peak}$ and w are the fitting parameters. By extrapolating $T_{\rm peak}$ to the infinite volume, we estimate the deconfining temperature $T_{\rm dec}(i\tilde{\theta})$ at each $\tilde{\theta}$.

The result of $T_{\rm dec}(i\tilde{\theta})/T_{\rm c}$ is plotted in figure 9 against $(\theta/\pi)^2 = -(\tilde{\theta}/\pi)^2$. Since the deconfining temperature is invariant under the CP transformation $\theta \to -\theta$, it should be an even function of θ. Here we fit our results for the deconfining temperature to

$$\frac{T_{\rm dec}(\theta)}{T_{\rm c}} = c_0 - c_2 \left(\frac{\theta}{\pi}\right)^2\,, \tag{4.7}$$

which yields[10] $c_0 = 1.0183(16)$, $c_2 = 0.225(12)$. The result of the fit is shown in figure 9, where we also extend the fitting function to the real θ region. Note that the vertical intercept of the fitting line being $c_0 \neq 1$ is not a contradiction since $T_{\rm c}$ represents the deconfining temperature in the continuum limit, whereas $T_{\rm dec}(\theta)$ is obtained at finite lattice spacing. While the prediction for the deconfining temperature $T_{\rm dec}(\theta)/T_{\rm c}$ in the real θ region depends much on the ansatz, we may safely conclude that $T_{\rm dec}(\theta) < T_{\rm c}$.

Having identified the deconfining phase transition line in the imaginary θ region, we can discuss how it affects the $\tilde{\theta}$ dependence of the topological charge density $\langle Q\rangle_{i\tilde{\theta}}/V_{\rm s}$ after the infinite volume extrapolation. Let us focus on the bottom two plots in figure 6. From figure 9, we find that the critical $\tilde{\theta}$ at which the deconfining phase transition occurs is $\tilde{\theta}_{\rm c}/\pi = 0.32(2)$ and $\tilde{\theta}_{\rm c}/\pi = 0.60(2)$, respectively, for $T/T_{\rm c} = 1.04$ and $T/T_{\rm c} = 1.10$. In fact, we do see some deviation from the fitting curve around $\tilde{\theta} = \tilde{\theta}_{\rm c}$, which might be due to the deconfining phase transition. Despite this subtlety, we find that the data points are nicely fitted to the analytic functions (4.4) and (4.5). Therefore our basic assumption that $\langle Q\rangle_\theta$ is not only continuous but also analytic across the deconfining phase transition seems to be valid to good accuracy at least in the imaginary θ region.

5 Summary and discussions

In this paper, we have investigated the spontaneous breaking of CP symmetry in four-dimensional pure Yang-Mills theory at $\theta = \pi$, which has attracted a lot of attention in recent years since the 't Hooft anomaly matching condition suggested a nontrivial phase structure. In fact, at large N, it is known that the CP symmetry at $\theta = \pi$ is spontaneously broken in the confined phase and it gets restored in the deconfined phase. However, a CP broken deconfined phase may appear at small N since it is allowed by the anomaly matching condition. The aim of this work is to investigate this possibility by numerical simulations.

[10] In the SU(3) case, it is found that the coefficient c_2 in the first ansatz is positive as well [53, 70–72].

JHEP05(2025)009

In order to circumvent the sign problem that occurs in ordinary Monte Carlo methods due to the θ term, we perform simulations at imaginary θ, where the sign problem is absent, and make an analytic continuation to real θ. As the order parameter of the spontaneous CP symmetry breaking, we calculate the expectation value of the topological charge $\langle Q \rangle$ at $\theta = \pi$ in this way. Our results suggest that the CP restoration temperature $T_{\rm CP}$ is very close to $T_{\rm c}$, which is the deconfining temperature at $\theta = 0$. We have also estimated the θ dependence of the deconfining temperature by analytic continuation and found that $T_{\rm dec}(\theta = \pi) < T_{\rm c}$. Combining these two results, we have concluded the existence of a CP broken deconfined phase at $\theta = \pi$, in striking contrast to the situation at large N.

Let us note that it is not straightforward to take the continuum limit by increasing the inverse coupling β since that will cause the so-called topology freezing problem. (See, however, ref. [79] and references therein for recent developments in solving this problem.) Instead, it would be worthwhile to improve the gauge action by including 1×2 Wilson loops, which will enable us to reduce the number of smearing steps. This is useful not only in reducing the possible artifacts of the stout smearing but also in reducing the computational cost, which will be important in increasing the lattice size.

We are currently trying to extend our work to the SU(3) YM theory, where the phase structure at $\theta = \pi$ is expected [28] to be like figure 1 (Left), similarly to the large-N case. Considering that $T_{\rm dec}(\pi) < T_{\rm c}$ is expected in SU(3) [53, 69–72] as well, we may find that $T_{\rm CP}$ is significantly lower than $T_{\rm c}$ unlike in the SU(2) case, where we have found $T_{\rm CP} \simeq T_{\rm c}$.

Acknowledgments

We would like to thank Kohta Hatakeyama for his participation at the earlier stage of this work. The authors are also grateful to Yuta Ito and Yuya Tanizaki for valuable discussions and comments. The computations were carried out on Yukawa-21 at YITP in Kyoto University and the PC clusters at KEK Computing Research Center and KEK Theory Center. This work also used computational resources of supercomputer NEC SX-Aurora TSUBASA provided by the Particle, Nuclear, and Astro Physics Simulation Program No.2020-009 (FY2020), No.2021-005 (FY2021), No.2022-004 (FY2022), and 2023-002(FY2023) of Institute of Particle and Nuclear Studies, High Energy Accelerator Research Organization (KEK). M. Honda is supported by JST PRESTO Grant Number JPMJPR2117, JST CREST Grant Number JPMJCR24I3, JSPS Grant-in-Aid for Transformative Research Areas (A) "Extreme Universe" JP21H05190 [D01] and JSPS KAKENHI Grant Number 22H01222. A. M. is supported by JSPS Grant-in-Aid for Transformative Research Areas (A) JP21H05190. A. Y. is supported by JSPS Grant-in-Aid for Transformative Research Areas (A) JP21H05191.

A Derivation of the HMC force term with the stout smearing

The stout smearing used in our simulation has been proposed in ref. [67] originally in the SU(3) case, and it has also been applied to the SU(2) case, for instance in refs. [80, 81]. Here we present the derivation of the HMC force term for the reader's convenience.

Let us consider the first smearing step

$$U_{n,\mu} \to U^{(1)}_{n,\mu} \equiv U'_{n,\mu} = e^{iY_{n,\mu}} U_{n,\mu} \,, \tag{A.1}$$

where $e^{iY_{n,\mu}}$ is defined by (3.6), and calculate the drift term $D^a_{n,\mu}S[U'(U)]$ for the original link variable, where the derivative is defined as

$$D^a_{n,\mu}F(U_{n,\mu}) \equiv \lim_{\epsilon\to 0}\frac{F(e^{i\epsilon\tau^a}U_{n,\mu}) - F(U_{n,\mu})}{\epsilon}\,, \tag{A.2}$$

where τ^a are the SU(2) generators with the normalization $\mathrm{tr}\left(\tau^a\tau^b\right) = \frac{1}{2}\delta_{ab}$. Note first that

$$U'_{m,\nu}\left(e^{i\alpha^a\tau^a}U_{n,\mu}\right) \approx \left\{\mathbb{1} + \alpha^a\left(D^a_{n,\mu}U'_{m,\nu}\right)(U'_{m,\nu})^\dagger\right\}U'_{m,\nu}\,, \tag{A.3}$$

up to the first order in α^a. The quantity in the parenthesis on the right-hand side can be rewritten as

$$\begin{aligned}\alpha^a\left(D^a_{n,\mu}U'_{m,\nu}\right)(U'_{m,\nu})^\dagger &= 2\alpha^a\mathrm{Tr}\left\{\left(D^a_{n,\mu}U'_{m,\nu}\right)(U'_{m,\nu})^\dagger\tau^b\right\}\tau^b \\ &= i\alpha^a\Delta^{a;b}_{n,\mu;m,\nu}\tau^b\,,\end{aligned} \tag{A.4}$$

where we have defined

$$\Delta^{a;b}_{n,\mu;m,\nu} \equiv -2i\mathrm{Tr}\left\{\left(D^a_{n,\mu}U'_{m,\nu}\right)(U'_{m,\nu})^\dagger\tau^b\right\}\,. \tag{A.5}$$

In deriving (A.4), we have used the identity

$$\mathrm{Tr}\left(W\tau^a\right)\tau^a = \frac{1}{2}\left\{W - \frac{1}{N}\mathrm{Tr}\left(W\right)\mathbb{1}\right\}\,, \tag{A.6}$$

in which the trace part on the right-hand side vanishes in the present case as

$$\begin{aligned}\mathrm{Tr}\left\{\left(D^a_{n,\mu}U'_{m,\nu}\right)(U'_{m,\nu})^\dagger\right\} &= \mathrm{Tr}\left\{D^a_{n,\mu}\left(e^{iY_{m,\nu}}U_{m,\nu}\right)U^\dagger_{m,\nu}e^{-iY_{m,\nu}}\right\} \\ &= \mathrm{Tr}\left(e^{-iY_{m,\nu}}D^a_{n,\mu}e^{iY_{m,\nu}} + U^\dagger_{m,\nu}D^a_{n,\mu}U_{m,\nu}\right) \\ &= i\mathrm{Tr}\left(D^a_{n,\mu}Y_{m,\nu}\right) + i\delta_{nm}\delta_{\mu\nu}\mathrm{Tr}\left(U^\dagger_{m,\nu}\tau^aU_{m,\nu}\right) \\ &= 0\,.\end{aligned} \tag{A.7}$$

Plugging (A.4) in (A.3), we obtain

$$\begin{aligned}U'_{m,\nu}\left(e^{i\alpha^a\tau^a}U_{n,\mu}\right) &= \left[\mathbb{1} + i\alpha^a\Delta^{a;b}_{n,\mu;m,\nu}\tau^b\right]U'_{m,\nu} \\ &\approx \exp\left(i\alpha^a\Delta^{a;b}_{n,\mu;m,\nu}\tau^b\right)U'_{m,\nu}\,.\end{aligned} \tag{A.8}$$

Thus we obtain the chain rule

$$D^a_{n,\mu}S\left[U'(U)\right] = \sum_{m,\nu}\Delta^{a;b}_{n,\mu;m,\nu}D'^b_{m,\nu}S\left[U'\right]\,, \tag{A.9}$$

where the primed derivative $D'^b_{m,\nu}$ is assumed to act on U'. The relation between the drift

$$F'_{n,\mu} \equiv i\tau^aD'^a_{n,\mu}S\left[U'(U)\right] \tag{A.10}$$

for the smeared link and the drift $F_{n,\mu}$ for the original link is obtained as

$$\begin{aligned}
F_{n,\mu} &\equiv i\tau^a D^a_{n,\mu} S\left[U'(U)\right] \\
&= i\tau^a \sum_{m,\nu} \Delta^{a;b}_{n,\mu;m,\nu} D'^b_{m,\nu} S\left[U'\right] \\
&= -2i\tau^a \sum_{m,\nu} \mathrm{Tr}\left[\left\{\left(D^a_{n,\mu} e^{iY_{m,\nu}}\right) e^{-iY_{m,\nu}} + e^{iY_{m,\nu}}\left(D^a_{n,\mu} U_{m,\nu}\right) U^\dagger_{m,\nu} e^{-iY_{m,\nu}}\right\} F'_{m,\nu}\right] \\
&= -2i\tau^a \sum_{m,\nu} \left\{\mathrm{Tr}\left[e^{-iY_{m,\nu}} F'_{m,\nu} D^a_{n,\mu} e^{iY_{m,\nu}}\right] + i\delta_{nm}\delta_{\mu\nu}\mathrm{Tr}\left[e^{iY_{m,\nu}}\tau^a e^{-iY_{m,\nu}} F'_{m,\nu}\right]\right\} \\
&= -2i\tau^a \sum_{m,\nu} \mathrm{Tr}\left[e^{-iY_{m,\nu}} F'_{m,\nu} D^a_{n,\mu} e^{iY_{m,\nu}}\right] + e^{-iY_{n,\mu}} F'_{n,\mu} e^{iY_{n,\mu}} \,. \qquad \text{(A.11)}
\end{aligned}$$

Let us recall that $e^{iY_{n,\mu}}$ can be written as (3.11) using (3.10). We rewrite (3.11) as

$$\exp(iY_{n,\mu}) = (\cos\kappa_{n,\mu})\mathbb{1} + i\, f(\kappa_{n,\mu})\, Y_{n,\mu}\,, \qquad \text{(A.12)}$$

using the analytic function $f(x)$ defined as[11]

$$f(x) = \frac{\sin x}{x} = 1 - x^2\left[\frac{1}{6} - x^2\left(\frac{1}{120} - \frac{x^2}{5040}\right)\right] + \mathrm{O}(x^8)\,. \qquad \text{(A.13)}$$

Using this function, the derivative in the first term in (A.11) is decomposed as

$$\begin{aligned}
\mathrm{Tr}\left(e^{-iY_{m,\nu}} F'_{m,\nu} D^a_{n,\mu} e^{iY_{m,\nu}}\right) &= \mathrm{Tr}\left[e^{-iY_{m,\nu}} F'_{m,\nu}\left\{-\sin\kappa_{m,\nu}\mathbb{1} + f'(\kappa_{m,\nu}) iY_{m,\nu}\right\}\right] D^a_{n,\mu}\kappa_{m,\nu} \\
&\quad + f(\kappa_{m,\nu})\mathrm{Tr}\left(e^{-iY_{m,\nu}} F'_{m,\nu} i D^a_{n,\mu} Y_{m,\nu}\right)\,. \qquad \text{(A.14)}
\end{aligned}$$

The first trace in (A.14) can be simplified by using the property $Y^2_{m,\nu} = \kappa^2_{m,\nu}\mathbb{1}$ of the 2×2 traceless matrix and $\mathrm{Tr}F'_{n,\mu} = 0$ as

$$\mathrm{Tr}\left[e^{-iY_{m,\nu}} F'_{m,\nu}\left\{-\sin\kappa_{m,\nu}\mathbb{1} + f'(\kappa_{m,\nu}) iY_{m,\nu}\right\}\right] = \frac{1 - f(2\kappa_{m,\nu})}{\kappa_{m,\nu}}\mathrm{Tr}\left(F'_{m,\nu} iY_{m,\nu}\right)\,. \qquad \text{(A.15)}$$

Converting the derivative of $\kappa_{m,\nu}$ to the derivative of $Y_{m,\nu}$ as

$$D^a_{n,\mu}\kappa_{m,\nu} = D^a_{n,\mu}\sqrt{\frac{1}{2}\mathrm{Tr}Y^2_{m,\nu}} = -\frac{1}{2\kappa_{m,\nu}}\mathrm{Tr}\left(iY_{m,\nu} iD^a_{n,\mu} Y_{m,\nu}\right)\,, \qquad \text{(A.16)}$$

all the derivatives in (A.14) can be written in terms of $D^a_{n,\mu}Y_{m,\nu}$ as

$$\begin{aligned}
&\mathrm{Tr}\left(e^{-iY_{m,\nu}} F'_{m,\nu} D^a_{n,\mu} e^{iY_{m,\nu}}\right) \\
&= -\frac{1 - f(2\kappa_{m,\nu})}{2\kappa^2_{m,\nu}}\mathrm{Tr}\left(F'_{m,\nu} iY_{m,\nu}\right)\mathrm{Tr}\left(iY_{m,\nu} iD^a_{n,\mu} Y_{m,\nu}\right) + f(\kappa_{m,\nu})\mathrm{Tr}\left(e^{-iY_{m,\nu}} F'_{m,\nu} iD^a_{n,\mu} Y_{m,\nu}\right) \\
&= \mathrm{Tr}\left[\left\{-\frac{1 - f(2\kappa_{m,\nu})}{2\kappa^2_{m,\nu}}\mathrm{Tr}\left(F'_{m,\nu} iY_{m,\nu}\right) iY_{m,\nu} + f(\kappa_{m,\nu}) e^{-iY_{m,\nu}} F'_{m,\nu}\right\} iD^a_{n,\mu} Y_{m,\nu}\right]\,. \qquad \text{(A.17)}
\end{aligned}$$

[11] The fact that the function $f(x)$ is analytic is important for using the stout smearing in the HMC algorithm.

JHEP05(2025)009

Plugging this in (A.11), we obtain the form of the drift term

$$F_{n,\mu} = -2i\tau^a \sum_{m,\nu} \mathrm{Tr}\left(\hat{\Lambda}_{m,\nu} i D^a_{n,\mu} Y_{m,\nu}\right) + e^{-iY_{n,\mu}} F'_{n,\mu} e^{iY_{n,\mu}} \,, \tag{A.18}$$

$$\hat{\Lambda}_{m,\nu} \equiv -\frac{1-f(2\kappa_{m,\nu})}{2\kappa^2_{m,\nu}} \mathrm{Tr}\left(F'_{m,\nu} i Y_{m,\nu}\right) i Y_{m,\nu} + f(\kappa_{m,\nu}) e^{-iY_{m,\nu}} F'_{m,\nu} \,. \tag{A.19}$$

Let us recall here that $Y_{m,\nu}$ is defined in terms of $J_{m,\nu}$ as (3.7). The first term of the left-hand side of (A.18) can be rewritten as

$$\begin{aligned} -2i\tau^a \sum_{m,\nu} \mathrm{Tr}\left(\hat{\Lambda}_{m,\nu} i D^a_{n,\mu} Y_{m,\nu}\right) &= 2i\rho\tau^a \sum_{m,\nu} \mathrm{Tr}\left\{\hat{\Lambda}_{m,\nu} \mathrm{Tr}\left(D^a_{n,\mu} J_{m,\nu} \tau^b\right) \tau^b\right\} \\ &= 2i\rho\tau^a \sum_{m,\nu} \mathrm{Tr}\left\{\mathrm{Tr}\left(\hat{\Lambda}_{m,\nu}\tau^b\right) \tau^b D^a_{n,\mu} J_{m,\nu}\right\} \\ &= 2i\rho\tau^a \sum_{m,\nu} \mathrm{Tr}\left(\Lambda_{m,\nu} D^a_{n,\mu} J_{m,\nu}\right) \,, \end{aligned} \tag{A.20}$$

where we have defined the traceless matrices

$$\Lambda_{m,\nu} \equiv \mathrm{Tr}\left(\hat{\Lambda}_{m,\nu}\tau^b\right)\tau^b = \frac{1}{2}\left\{\hat{\Lambda}_{m,\nu} - \frac{1}{2}\mathrm{Tr}\left(\hat{\Lambda}_{m,\nu}\right)\right\} \,. \tag{A.21}$$

Therefore the drift term

$$F_{n,\mu} = e^{-iY_{n,\mu}} F'_{n,\mu} e^{iY_{n,\mu}} + 2i\rho\tau^a \sum_{m,\nu} \mathrm{Tr}\left[\Lambda_{m,\nu} D^a_{n,\mu} J_{m,\nu}\right] \tag{A.22}$$

is obtained by calculating the derivative of the $J_{m,\nu}$, which is given by

$$\begin{aligned} D^a_{n,\mu} J_{m,\nu} &= D^a_{n,\mu}(U_{m,\nu}\Omega_{m,\nu} - \Omega^\dagger_{m,\nu} U^\dagger_{m,\nu}) \\ &= i\delta_{n,m}\delta_{\mu\nu}(\tau^a U_{m,\nu}\Omega_{m,\nu} + \Omega^\dagger_{m,\nu} U^\dagger_{m,\nu}\tau^a) + U_{m,\nu}(D^a_{n,\mu}\Omega_{m,\nu}) - (D^a_{n,\mu}\Omega^\dagger_{m,\nu}) U^\dagger_{m,\nu} \,, \end{aligned} \tag{A.23}$$

$$\begin{aligned} D^a_{n,\mu}\Omega_{m,\nu} &= i\,(1-\delta_{\mu\nu})\Big(\delta_{n,m+\nu}\tau^a U_{n,\mu} U^\dagger_{n+\mu-\nu,\nu} U^\dagger_{n-\nu,\mu} - \delta_{n,m} U_{n+\nu,\mu} U^\dagger_{n+\mu,\nu} U^\dagger_{n,\mu}\tau^a \\ &\qquad - \delta_{n,m+\nu-\mu} U^\dagger_{n,\mu}\tau^a U^\dagger_{n-\nu,\nu} U_{n-\nu,\mu} + \delta_{n,m-\mu} U^\dagger_{n+\nu,\mu} U^\dagger_{n,\nu}\tau^a U_{n,\mu}\Big) \\ &\quad - i\delta_{\mu\nu} \sum_{\sigma(\neq\mu)} \Big(\delta_{n,m+\sigma} U_{n+\mu-\sigma,\sigma} U^\dagger_{n,\mu}\tau^a U^\dagger_{n-\sigma,\sigma} + \delta_{n,m-\sigma} U^\dagger_{n+\mu,\sigma} U^\dagger_{n,\mu}\tau^a U_{n,\sigma}\Big) \,, \end{aligned} \tag{A.24}$$

$$\begin{aligned} D^a_{n,\mu}\Omega^\dagger_{m,\nu} &= i\,(1-\delta_{\mu\nu})\Big(\delta_{n,m}\tau^a U_{n,\mu} U_{n+\mu,\nu} U^\dagger_{n+\nu,\mu} - \delta_{n,m+\nu} U_{n-\nu,\mu} U_{n+\mu-\nu,\nu} U^\dagger_{n,\mu}\tau^a \\ &\qquad - \delta_{n,m-\mu} U^\dagger_{n,\mu}\tau^a U_{n,\nu} U_{n+\nu,\mu} + \delta_{n,m+\nu-\mu} U^\dagger_{n-\nu,\mu} U_{n-\nu,\nu}\tau^a U_{n,\mu}\Big) \\ &\quad + i\delta_{\mu\nu} \sum_{\sigma(\neq\mu)} \Big(\delta_{n,m+\sigma} U_{n-\sigma,\sigma}\tau^a U_{n,\mu} U^\dagger_{n+\mu-\sigma,\sigma} + \delta_{n,m-\sigma} U^\dagger_{n,\sigma}\tau^a U_{n,\mu} U_{n+\mu,\sigma}\Big) \,. \end{aligned} \tag{A.25}$$

Data Availability Statement. This article has no associated data or the data will not be deposited.

Code Availability Statement. This article has no associated code or the code will not be deposited.

JHEP05(2025)009

References

[1] I. Affleck and F.D.M. Haldane, *Critical theory of quantum spin chains*, *Phys. Rev. B* **36** (1987) 5291 [INSPIRE].

[2] R. Shankar and N. Read, *The $\theta = \pi$ nonlinear σ model is massless*, *Nucl. Phys. B* **336** (1990) 457 [INSPIRE].

[3] Y. Kato and A. Tanaka, *Numerical study of the $S = 1$ antiferromagnetic spin chain with bond alternation*, *J. Phys. Soc. Jpn.* **63** (1994) 1277 [cond-mat/9401053].

[4] W. Bietenholz, A. Pochinsky and U.J. Wiese, *Meron cluster simulation of the theta vacuum in the 2d O(3) model*, *Phys. Rev. Lett.* **75** (1995) 4524 [hep-lat/9505019] [INSPIRE].

[5] M. Yamanaka, M. Oshikawa and S. Miyashita, *Hidden order and dimerization transition in $S = 2$ chains*, *J. Phys. Soc. Jpn.* **65** (1996) 1562 [cond-mat/9604107].

[6] B. Alles and A. Papa, *Mass gap in the 2D O(3) non-linear sigma model with a $\theta = \pi$ term*, *Phys. Rev. D* **77** (2008) 056008 [arXiv:0711.1496] [INSPIRE].

[7] M. Bogli, F. Niedermayer, M. Pepe and U.J. Wiese, *Non-trivial θ-vacuum effects in the 2d O(3) model*, *JHEP* **04** (2012) 117 [arXiv:1112.1873] [INSPIRE].

[8] P. de Forcrand, M. Pepe and U.-J. Wiese, *Walking near a conformal fixed point: The 2d O(3) model at θ near π as a test case*, *Phys. Rev. D* **86** (2012) 075006 [arXiv:1204.4913] [INSPIRE].

[9] B. Alles, M. Giordano and A. Papa, *Behavior near $\theta = \pi$ of the mass gap in the two-dimensional O(3) non-linear sigma model*, *Phys. Rev. B* **90** (2014) 184421 [arXiv:1409.1704] [INSPIRE].

[10] W. Tang, X.C. Xie, L. Wang and H.-H. Tu, *Tensor network simulation of the (1+1)-dimensional O(3) nonlinear σ-model with $\theta = \pi$ term*, *Phys. Rev. D* **104** (2021) 114513 [arXiv:2109.11324] [INSPIRE].

[11] F.D.M. Haldane, *Nonlinear field theory of large spin Heisenberg antiferromagnets: Semiclassically quantized solitons of the one-dimensional easy-axis Néel state*, *Phys. Rev. Lett.* **50** (1983) 1153 [INSPIRE].

[12] F.D.M. Haldane, *Continuum dynamics of the 1D Heisenberg antiferromagnetic: Identification with the O(3) nonlinear sigma model*, *Phys. Lett. A* **93** (1983) 464 [INSPIRE].

[13] C.A. Baker et al., *An improved experimental limit on the electric dipole moment of the neutron*, *Phys. Rev. Lett.* **97** (2006) 131801 [hep-ex/0602020] [INSPIRE].

[14] C. Abel et al., *Measurement of the permanent electric dipole moment of the neutron*, *Phys. Rev. Lett.* **124** (2020) 081803 [arXiv:2001.11966] [INSPIRE].

[15] R.D. Peccei and H.R. Quinn, *CP conservation in the presence of instantons*, *Phys. Rev. Lett.* **38** (1977) 1440 [INSPIRE].

[16] R.D. Peccei and H.R. Quinn, *Constraints imposed by CP conservation in the presence of instantons*, *Phys. Rev. D* **16** (1977) 1791 [INSPIRE].

[17] S. Weinberg, *A new light boson?*, *Phys. Rev. Lett.* **40** (1978) 223 [INSPIRE].

[18] F. Wilczek, *Problem of strong P and T invariance in the presence of instantons*, *Phys. Rev. Lett.* **40** (1978) 279 [INSPIRE].

JHEP05(2025)009

[19] A.E. Nelson, *Naturally weak CP violation*, *Phys. Lett. B* **136** (1984) 387 [INSPIRE].

[20] S.M. Barr, *Solving the strong CP problem without the Peccei-Quinn symmetry*, *Phys. Rev. Lett.* **53** (1984) 329 [INSPIRE].

[21] W.-Y. Ai, J.S. Cruz, B. Garbrecht and C. Tamarit, *Consequences of the order of the limit of infinite spacetime volume and the sum over topological sectors for CP violation in the strong interactions*, *Phys. Lett. B* **822** (2021) 136616 [arXiv:2001.07152] [INSPIRE].

[22] W.-Y. Ai, B. Garbrecht and C. Tamarit, *CP conservation in the strong interactions*, *Universe* **10** (2024) 189 [arXiv:2404.16026] [INSPIRE].

[23] G. Schierholz, *Absence of strong CP violation*, *J. Phys. G* **52** (2025) 04LT01 [arXiv:2403.13508] [INSPIRE].

[24] D.J. Gross, R.D. Pisarski and L.G. Yaffe, *QCD and instantons at finite temperature*, *Rev. Mod. Phys.* **53** (1981) 43 [INSPIRE].

[25] N. Weiss, *The effective potential for the order parameter of gauge theories at finite temperature*, *Phys. Rev. D* **24** (1981) 475 [INSPIRE].

[26] D. Gaiotto, A. Kapustin, N. Seiberg and B. Willett, *Generalized global symmetries*, *JHEP* **02** (2015) 172 [arXiv:1412.5148] [INSPIRE].

[27] G. 't Hooft, *Naturalness, chiral symmetry, and spontaneous chiral symmetry breaking*, *NATO Sci. Ser. B* **59** (1980) 135 [INSPIRE].

[28] D. Gaiotto, A. Kapustin, Z. Komargodski and N. Seiberg, *Theta, time reversal, and temperature*, *JHEP* **05** (2017) 091 [arXiv:1703.00501] [INSPIRE].

[29] C. Córdova and K. Ohmori, *Anomaly obstructions to symmetry preserving gapped phases*, arXiv:1910.04962 [INSPIRE].

[30] E. Witten, *Large N chiral dynamics*, *Annals Phys.* **128** (1980) 363 [INSPIRE].

[31] E. Witten, *Theta dependence in the large N limit of four-dimensional gauge theories*, *Phys. Rev. Lett.* **81** (1998) 2862 [hep-th/9807109] [INSPIRE].

[32] S. Chen, K. Fukushima, H. Nishimura and Y. Tanizaki, *Deconfinement and CP breaking at $\theta = \pi$ in Yang-Mills theories and a novel phase for SU(2)*, *Phys. Rev. D* **102** (2020) 034020 [arXiv:2006.01487] [INSPIRE].

[33] M. Hanada, J. Holden, M. Knaggs and A. O'Bannon, *Global symmetries and partial confinement*, *JHEP* **03** (2022) 118 [arXiv:2112.11398] [INSPIRE].

[34] R. Kitano, N. Yamada and M. Yamazaki, *Is $N = 2$ large?*, *JHEP* **02** (2021) 073 [arXiv:2010.08810] [INSPIRE].

[35] R. Kitano, R. Matsudo, N. Yamada and M. Yamazaki, *Peeking into the θ vacuum*, *Phys. Lett. B* **822** (2021) 136657 [arXiv:2102.08784] [INSPIRE].

[36] N. Yamada, M. Yamazaki and R. Kitano, *Subvolume method for SU(2) Yang-Mills theory at finite temperature: topological charge distributions*, *JHEP* **07** (2024) 198 [arXiv:2403.10767] [INSPIRE].

[37] C. Gattringer and O. Orasch, *Density of states approach for lattice gauge theory with a θ-term*, *Nucl. Phys. B* **957** (2020) 115097 [arXiv:2004.03837] [INSPIRE].

[38] M. Hirasawa, A. Matsumoto, J. Nishimura and A. Yosprakob, *Complex Langevin analysis of 2D U(1) gauge theory on a torus with a θ term*, *JHEP* **09** (2020) 023 [arXiv:2004.13982] [INSPIRE].

JHEP05(2025)009

[39] C. Gattringer and O. Orasch, *Density of states approach for lattice field theory with topological terms*, *PoS* **LATTICE2021** (2022) 158 [arXiv:2111.09535] [INSPIRE].

[40] A. Matsumoto et al., *A new technique for solving the freezing problem in the complex Langevin simulation of 4D SU(2) gauge theory with a theta term*, *PoS* **LATTICE2021** (2022) 087 [arXiv:2112.01805] [INSPIRE].

[41] L. Bongiovanni, G. Aarts, E. Seiler and D. Sexty, *Complex Langevin dynamics for SU(3) gauge theory in the presence of a theta term*, *PoS* **LATTICE2014** (2014) 199 [arXiv:1411.0949] [INSPIRE].

[42] Y. Kuramashi and Y. Yoshimura, *Tensor renormalization group study of two-dimensional U(1) lattice gauge theory with a θ term*, *JHEP* **04** (2020) 089 [arXiv:1911.06480] [INSPIRE].

[43] M. Hirasawa, A. Matsumoto, J. Nishimura and A. Yosprakob, *Tensor renormalization group and the volume independence in 2D U(N) and SU(N) gauge theories*, *JHEP* **12** (2021) 011 [arXiv:2110.05800] [INSPIRE].

[44] M. Fukuma, D. Kadoh and N. Matsumoto, *Tensor network approach to two-dimensional Yang-Mills theories*, *PTEP* **2021** (2021) 123B03 [arXiv:2107.14149] [INSPIRE].

[45] M. Asaduzzaman et al., *Tensor network representation of non-Abelian gauge theory coupled to reduced staggered fermions*, *JHEP* **05** (2024) 195 [arXiv:2312.16167] [INSPIRE].

[46] T. Kuwahara and A. Tsuchiya, *Toward tensor renormalization group study of three-dimensional non-Abelian gauge theory*, *PTEP* **2022** (2022) 093B02 [arXiv:2205.08883] [INSPIRE].

[47] A. Yosprakob, *Reduced tensor network formulation for non-Abelian gauge theories in arbitrary dimensions*, *PTEP* **2024** (2024) 073B05 [arXiv:2311.02541] [INSPIRE].

[48] A. Yosprakob and K. Okunishi, *Tensor renormalization group study of the 3D SU(2) and SU(3) gauge theories with the reduced tensor network formulation*, *PTEP* **2025** (2025) 033B06 [arXiv:2406.16763] [INSPIRE].

[49] M. Berni, C. Bonanno and M. D'Elia, *Large-N expansion and θ-dependence of 2d CP^{N-1} models beyond the leading order*, *Phys. Rev. D* **100** (2019) 114509 [arXiv:1911.03384] [INSPIRE].

[50] P. de Forcrand and O. Philipsen, *The QCD phase diagram for small densities from imaginary chemical potential*, *Nucl. Phys. B* **642** (2002) 290 [hep-lat/0205016] [INSPIRE].

[51] M. D'Elia and M.-P. Lombardo, *Finite density QCD via imaginary chemical potential*, *Phys. Rev. D* **67** (2003) 014505 [hep-lat/0209146] [INSPIRE].

[52] M. D'Elia and F. Negro, *θ dependence of the deconfinement temperature in Yang-Mills theories*, *Phys. Rev. Lett.* **109** (2012) 072001 [arXiv:1205.0538] [INSPIRE].

[53] M. D'Elia and F. Negro, *Phase diagram of Yang-Mills theories in the presence of a θ term*, *Phys. Rev. D* **88** (2013) 034503 [arXiv:1306.2919] [INSPIRE].

[54] C. Bonanno, M. D'Elia and L. Verzichelli, *The θ-dependence of the SU(N) critical temperature at large N*, *JHEP* **02** (2024) 156 [arXiv:2312.12202] [INSPIRE].

[55] H. Panagopoulos and E. Vicari, *The 4D SU(3) gauge theory with an imaginary θ term*, *JHEP* **11** (2011) 119 [arXiv:1109.6815] [INSPIRE].

[56] C. Bonati, M. D'Elia and A. Scapellato, *θ dependence in SU(3) Yang-Mills theory from analytic continuation*, *Phys. Rev. D* **93** (2016) 025028 [arXiv:1512.01544] [INSPIRE].

[57] C. Bonati, M. D'Elia, P. Rossi and E. Vicari, *θ dependence of 4D SU(N) gauge theories in the large-N limit*, *Phys. Rev. D* **94** (2016) 085017 [arXiv:1607.06360] [INSPIRE].

JHEP05(2025)009

[58] C. Bonanno, C. Bonati, M. Papace and D. Vadacchino, *The θ-dependence of the Yang-Mills spectrum from analytic continuation*, *JHEP* **05** (2024) 163 [arXiv:2402.03096] [INSPIRE].

[59] S. Aoki et al., *The electric dipole moment of the nucleon from simulations at imaginary vacuum angle theta*, arXiv:0808.1428 [INSPIRE].

[60] F.-K. Guo et al., *The electric dipole moment of the neutron from 2+1 flavor lattice QCD*, *Phys. Rev. Lett.* **115** (2015) 062001 [arXiv:1502.02295] [INSPIRE].

[61] V. Azcoiti, G. Di Carlo, A. Galante and V. Laliena, *New proposal for numerical simulations of theta vacuum-like systems*, *Phys. Rev. Lett.* **89** (2002) 141601 [hep-lat/0203017] [INSPIRE].

[62] V. Azcoiti, G. Di Carlo, A. Galante and V. Laliena, *θ-vacuum systems via real action simulations*, *Phys. Lett. B* **563** (2003) 117 [hep-lat/0305005] [INSPIRE].

[63] V. Azcoiti et al., *Massive Schwinger model at finite θ*, *Phys. Rev. D* **97** (2018) 014507 [arXiv:1709.07667] [INSPIRE].

[64] V. Azcoiti, G. Di Carlo, A. Galante and V. Laliena, *θ dependence of CP^9 model*, *Phys. Rev. D* **69** (2004) 056006 [hep-lat/0305022] [INSPIRE].

[65] M. Imachi, M. Kambayashi, Y. Shinno and H. Yoneyama, *The θ-term, CP^{N-1} model and the inversion approach in the imaginary θ method*, *Prog. Theor. Phys.* **116** (2006) 181 [hep-lat/0601028] [INSPIRE].

[66] V. Azcoiti, G. Di Carlo and A. Galante, *Critical behaviour of CP^1 at $\theta = \pi$, Haldane's conjecture, and the relevant universality class*, *Phys. Rev. Lett.* **98** (2007) 257203 [arXiv:0710.1507] [INSPIRE].

[67] C. Morningstar and M.J. Peardon, *Analytic smearing of SU(3) link variables in lattice QCD*, *Phys. Rev. D* **69** (2004) 054501 [hep-lat/0311018] [INSPIRE].

[68] M. Unsal, *Theta dependence, sign problems and topological interference*, *Phys. Rev. D* **86** (2012) 105012 [arXiv:1201.6426] [INSPIRE].

[69] E. Poppitz, T. Schäfer and M. Ünsal, *Universal mechanism of (semi-classical) deconfinement and theta-dependence for all simple groups*, *JHEP* **03** (2013) 087 [arXiv:1212.1238] [INSPIRE].

[70] M.M. Anber, *Θ dependence of the deconfining phase transition in pure $SU(N_c)$ Yang-Mills theories*, *Phys. Rev. D* **88** (2013) 085003 [arXiv:1302.2641] [INSPIRE].

[71] N. Otake and N. Yamada, *θ dependence of T_c in 4d $SU(3)$ Yang-Mills theory with histogram method and the Lee-Yang zeros in the large N limit*, *JHEP* **06** (2022) 044 [arXiv:2202.05605] [INSPIRE].

[72] S. Borsanyi et al., *Topological features of the deconfinement transition*, *Phys. Rev. D* **107** (2023) 054514 [arXiv:2212.08684] [INSPIRE].

[73] J. Engels, F. Karsch and K. Redlich, *Scaling properties of the energy density in SU(2) lattice gauge theory*, *Nucl. Phys. B* **435** (1995) 295 [hep-lat/9408009] [INSPIRE].

[74] P. Di Vecchia, K. Fabricius, G.C. Rossi and G. Veneziano, *Preliminary evidence for $U(1)_A$ breaking in QCD from lattice calculations*, *Nucl. Phys. B* **192** (1981) 392 [INSPIRE].

[75] M. Lüscher, *Properties and uses of the Wilson flow in lattice QCD*, *JHEP* **08** (2010) 071 [*Erratum ibid.* **03** (2014) 092] [arXiv:1006.4518] [INSPIRE].

[76] L. Del Debbio, H. Panagopoulos and E. Vicari, *θ dependence of SU(N) gauge theories*, *JHEP* **08** (2002) 044 [hep-th/0204125] [INSPIRE].

JHEP05(2025)009

[77] S. Durr, Z. Fodor, C. Hoelbling and T. Kurth, *Precision study of the SU(3) topological susceptibility in the continuum*, *JHEP* **04** (2007) 055 [hep-lat/0612021] [INSPIRE].

[78] N. Yamada, M. Yamazaki and R. Kitano, *θ dependence of T_c in $SU(2)$ Yang-Mills theory*, *JHEP* **02** (2025) 211 [arXiv:2411.00375] [INSPIRE].

[79] T. Eichhorn, G. Fuwa, C. Hoelbling and L. Varnhorst, *Parallel tempered metadynamics: Overcoming potential barriers without surfing or tunneling*, *Phys. Rev. D* **109** (2024) 114504 [arXiv:2307.04742] [INSPIRE].

[80] A. Hasenfratz, R. Hoffmann and S. Schaefer, *Hypercubic smeared links for dynamical fermions*, *JHEP* **05** (2007) 029 [hep-lat/0702028] [INSPIRE].

[81] S. Catterall and A. Veernala, *Four fermion interactions in non-Abelian gauge theory*, *Phys. Rev. D* **87** (2013) 114507 [arXiv:1303.6187] [INSPIRE].

JHEP05(2025)009